Published in final edited form as:
Mol Pharm. 2011 April 4; 8(2): 621–628. doi:10.1021/mp100446t.

Multiplexed PET Probes for Imaging Breast Cancer Early Response to $VEGF_{121}$/rGel Treatment

Min Yang[1,2,†], **Haokao Gao**[2,3,†], **Xilin Sun**[2], **Yongjun Yan**[2], **Qimeng Quan**[2], **Wendy Zhang**[4], **Khalid Mohamedali**[4], **Michael G. Rosenblum**[4], **Gang Niu**[2,*], and **Xiaoyuan Chen**[2,*]

[1]Key Laboratory of Nuclear Medicine, Ministry of Health, Jiangsu Key Laboratory of Molecular Nuclear Medicine, Jiangsu Institute of Nuclear Medicine. Wuxi, Jiangsu 214063, China

[2]Laboratory of Molecular Imaging and Nanomedicine (LOMIN), National Institute of Biomedical Imaging and Bioengineering (NIBIB), National Institutes of Health (NIH), Bethesda, MD 20892-2281, USA

[3]Department of Cardiology, Xijing Hospital, the Fourth Military Medical University, Xian 710032, China

[4]Department of Experimental Therapeutics, UT MD Anderson Cancer Center, Houston, TX 77030, USA

Abstract

In this study, we applied multiplexed positron emission tomography (PET) probes to monitor glucose metabolism, cellular proliferation, tumor hypoxia and angiogenesis during $VEGF_{121}$/rGel therapy of breast cancer. Two doses of 12 mg/kg $VEGF_{121}$/rGel, administered intraperitoneally, resulted in initial delay of tumor growth, but the growth resumed 4 days after tumor treatment was stopped. The average tumor growth rate expressed as V/V_0, were 1.11 ± 0.07, 1.21 ± 0.10, 1.58 ± 0.36 and 2.64 ± 0.72 at days 1, 3, 7 and 14, respectively. Meanwhile, the $VEGF_{121}$/rGel treatment group showed V/V_0 ratios of 1.04 ± 0.06, 1.05 ± 0.11, 1.09 ± 0.17 and 1.86 ± 0.36 at days 1, 3, 7 and 14, respectively. $VEGF_{121}$/rGel treatment led to significantly decreased uptake of ^{18}F-FPPRGD2 at day 1 (24.0 ± 8.8%, $p < 0.05$) and day 3 (36.3 ± 9.2%, $p < 0.01$), relative to the baseline, which slowly recovered to the baseline at day 14. ^{18}F-FMISO uptake was increased in the treated tumors at day 1 (23.9 ± 15.7%, $p < 0.05$) and day 3 (51.4 ± 29.4%, $p < 0.01$), as compared to the control group. At day 7 and 14, ^{18}F-FMISO uptake restored to the baseline level. The relative reductions in FLT uptake in treated tumors were approximately 13.0 ± 4.5% at day 1 and 25.0 ± 4.4% ($p < 0.01$) at day 3. No significant change of ^{18}F-FDG uptake was observed in $VEGF_{121}$/rGel treated tumors, compared with the control group. The imaging findings were supported by *ex vivo* analysis of related biomarkers. Overall, longitudinal imaging studies with 4 PET tracers demonstrated the feasibility and usefulness of multiplexed probes for quantitative measurement of anti-tumor effects of $VEGF_{121}$/rGel at the early stage of treatment. This pre-clinical study should be helpful in accelerating anti-cancer drug development and promoting the clinical translation of molecular imaging.

Keywords

positron emission tomography (PET); ^{18}F-FDG; ^{18}F-FLT; ^{18}F-FPPRGD2; ^{18}F-FMISO; integrin; therapy response

[*]**Correspondence:** Gang Niu, niug@mail.nih.gov; Xiaoyuan Chen, shawn.chen@nih.gov.
[†]These authors contributed equally in this work.

Introduction

Monitoring of tumor early response to therapy is important in clinical oncology to reduce side effects and save costs, especially with the growing number of alternative treatment regimens that are only effective in select subgroups of patients.[1] The traditional approach to monitoring treatment through imaging has relied on assessing the change of tumor size before and after treatment using refined criteria defined by the World Health Organization (WHO) criteria and more recently by the Response Evaluation Criteria in Solid Tumors (RECIST).[2–3] However, many new anti-angiogenic drugs are principally cytostatic and do not necessarily cause large reductions in tumor volume on a short timescale, even when they are effective, which reduces the usefulness of anatomic measures in monitoring response to such agents.4 Thus, new imaging biomarkers of tumor response that correlate better with therapeutic outcomes are urgently needed.1

$VEGF_{121}$/rGel fusion protein is a vascular disruptive agent composed of the VEGF-A isoform $VEGF_{121}$ and recombinant plant toxin gelonin (rGel).[5] This novel vasculature-targeting fusion protein has high specificity and cytotoxicity for both quiescent and dividing porcine aortic endothelial (PAE) cells expressing VEGFR-2 (PAE/KDR), but not for PAE cells expressing VEGFR-1 (PAE/FLT-1).5 $VEGF_{121}$/rGel has been shown to completely suppress ocular neovascularization[6] and inhibit the growth of melanoma and glioblastoma, as well as prostate, breast, and bladder tumor models with low systemic toxicity.[5, 7–8] A critical step in future clinical application of $VEGF_{121}$/rGel and other antiangiogenic therapies is to develop effective noninvasive *in vivo* imaging techniques to monitor treatment efficacy. In a previous study, we evaluated the antiangiogenic and antitumor effects of $VEGF_{121}$/rGel in an orthotopic glioblastoma mouse model by using bioluminescence imaging (BLI), MRI, and PET.[8] Indeed, PET with ^{18}F-FLT revealed significant decreases in tumor proliferation in $VEGF_{121}$/rGel-treated mice compared with the control mice.

Tumor response to therapeutics is an extremely complicated process, even though therapy might aim at a particular target or specific pathway. PET with the glucose analog ^{18}F-FDG is currently the more clinically advanced than several other functional/molecular imaging approaches for treatment monitoring, including dynamic contrast-enhanced MRI, diffusion-weighted MRI, MR spectroscopy, optical imaging, and contrast-enhanced ultrasound.[9] However, FDG PET reflects metabolic changes and, in addition to the effects of treatment, it is also affected by other factors including inflammation, hypoxia and serum glucose level.[4] Consequently, imaging probes targeting DNA synthesis, hypoxia, and angiogenesis are expected to complement ^{18}F-FDG in treatment monitoring by providing more specific information on the biological effects of therapeutic agents. In this study, using ^{18}F-FDG, ^{18}F-FLT, ^{18}F-FMISO, and ^{18}F-FPPRGD2 as imaging probes, we applied multiplexed PET imaging to evaluate tumor response to $VEGF_{121}$/rGel treatment in an orthotopic MDA-MB-435 breast cancer model.

Experimental Section

General Materials

Unless otherwise specified, all reagents were of analytical grade and were obtained from commercial sources. $VEGF_{121}$/rGel was obtained as previously described.[8] ^{18}F-F^- radionuclide was obtained from the NIH Clinical Center's cyclotron facility by proton irradiation of ^{18}O-enriched water. ^{18}F-FDG was purchased from the Nuclear Pharmacy of Cardinal Health, and reconstituted with sterile saline. Reversed-phase extraction C_{18} Sep-Pak cartridges were obtained from Waters Inc. and pretreated with ethanol and water before use. The syringe filter and polyethersulfone membranes (pore size, 0.22 mm; diameter, 13

mm) were obtained from Nalge Nunc International. Analytical as well as semi-preparative reversed-phase high-performance liquid chromatography (RP-HPLC) were performed on a Waters 600 chromatography system with a Waters 996 photodiode array detector and Beckman170 radioisotope detector. The recorded data were processed using Empower software.

Synthesis of ^{18}F-FLT, ^{18}F-FMISO and ^{18}F-FPPRGD2

^{18}F-FLT, ^{18}F-FMISO and ^{18}F-FPPRGD2 were prepared manually according to previous reports.[10–12] For purification of ^{18}F-FLT or ^{18}F-FMISO, a semi-preparative C_{18} HPLC column (Phenomenex Nucleosil C_{18} column, 108005; 5 mm, 300 × 10 mm) was eluted with 8% ethanol/H_2O (4 ml/min). The total synthesis time was about 40 min for each tracer. Radiochemical yields (decay uncorrected) for ^{18}F-FLT and ^{18}F-FMISO were 64.6 ± 8.3%, 70.5 ± 5.9%, respectively (n = 4).

For ^{18}F-FPPRGD2, the first step was to prepare purified and dried ^{18}F-NFP (radiochemical yield was 46.1 ± 6.9%, n = 4). Then ^{18}F-NFP and PRGD2 (0.1 μmol) were mixed at 105°C for 10 min. The mixture was purified by semi-preparative HPLC (218TP510, Vydac). The desired ^{18}F-FPPRGD2 fractions were combined and evaporated to dryness.

The three ^{18}F-labeled tracers were formulated in normal saline and passed through a 0.22 μm Millipore filter for animal use. The radiochemical purity was greater than 99% and specific activity was greater than 50TBq/mmol at the end of synthesis for each tracer.

Tumor growth, drug treatment and PET imaging

The MDA-MB-435 cell line was purchased from the American Type Culture Collection (ATCC) and grown in Leibovitz's L-15 medium supplemented with 10% (v/v) fetal bovine serum (FBS) under a 100% air atmosphere at 37 °C. The tumor model was developed in 5–6 week-old female athymic nude mice (Harlan Laboratories) by orthotopic injection of 5×10^6 cells in the left mammary fat pad of each mouse. Tumor growth was followed by perpendicular measures of the tumor using a caliper. The tumor volume was estimated by the formula: tumor volume = a× (b^2) / 2, where a and b were the tumor length and width, respectively, in millimeters. Once the tumor volumes reached approximately 200 mm^3, mice were randomized into treatment (n = 20) and control groups (n = 20). A maximum tolerated dose (MTD) of 45 mg/kg for $VEGF_{121}$/rGel was previously reported,[13] and 25% of the MTD was used in this study (12 mg/kg administered every other day for a total of 2 doses). PBS was used as the control vehicle. All procedures of this animal study were conducted under a protocol approved by the NIH Clinical Center Animal Care and Use Committee. All mice were maintained in a specific pathogen-free facility in accordance with the Institutional Animal Care and Use Committee of NIH.

The detailed therapy and longitudinal scan schedules are shown in Table 1. The animal numbers for each imaging protocol were 10, 9, 8, 7, 6 at day 0, 1, 3, 7 and 14 after treatment due to the loss from tumor tissue sampling. PET scans and image analysis were performed using an Inveon microPET scanner (Siemens Medical Solutions). Each MDA-MB-435 tumor-bearing mouse, under isoflurane anesthesia, was injected *via* tail vein with 1.11 MBq (30 μCi) of the first tracer (^{18}F-FPPRGD2 or ^{18}F-FMISO), then after 8 h interval with 1.85 MBq (50 μCi) of the second tracer (^{18}F-FDG or ^{18}F-FLT). Five-min static scans were acquired at 1 h (^{18}F-FPPRGD2, ^{18}F-FDG), 1.5 h (^{18}F-FLT) or 2.5 h (^{18}F-FMISO) after injection based on previous experience.[14–16] For the ^{18}F-FDG scan, mice were fasted for 6 h before tracer injection and were then maintained under isoflurane anesthesia during the injection, accumulation, and scanning periods.

The images were reconstructed using a two-dimensional ordered-subset expectation maximum (OSEM) algorithm, and no correction was applied for attenuation or scatter. For each microPET scan, regions of interest (ROIs) were drawn over the tumor using vendor software ASI Pro 5.2.4.0 on decay-corrected whole-body coronal images. The maximum radioactivity concentrations (accumulation) within a tumor were obtained from mean pixel values within the multiple ROI volume and then converted to megabecquerels (MBq) per milliliter per minute using a conversion factor. These values were then divided by the administered activity to obtain (assuming a tissue density of 1 g/ml) an image-ROI-derived percent injected dose per gram (ID%/g). Uptake ratios were then calculated by dividing the maximum value of pixels within a tumor ROI by the average value of pixels within the background ROI. The resolution of the Inveon microPET scanner was 1.4 mm and the average tumor diameter for all groups of animals was greater than 4 mm on all imaging days; therefore correction for partial volume effect was not required.

Fluorescence staining and image analysis

Tumor samples were collected at different time points as shown in Table 1. Frozen tumor tissue slices (5 μm) were fixed with cold acetone for 20 min and dried in the air for 30 min at room temperature. After blocking with 2% BSA for 30 min, the sections were incubated with primary antibody for 2 h at room temperature and then visualized with dye-conjugated secondary antibodies (1:400; Jackson ImmunoResearch Laboratories, West Grove, PA). The following primary antibodies against different target antigens were used: humanized anti-human integrin αvβ3 antibody (Abegrin, 1:200); rat anti-mouse CD31 antibody (1:300; BD Biosciences), hamster anti-mouse β3 CD61 antibody (1:200; BD Biosciences); rabbit anti-human Ki76 antibody (1:100; BD Biosciences); rabbit anti-human GLUT-1 antibody (1:300; Abcam, Inc.); rat anti-mouse F4/80 antibody (1:300; Abcam, Inc.). After washing 3 × 5 min with PBS, the whole slides were mounted with 4'-6-diamidino-2-phenylindole (DAPI)-containing mounting medium. Fluorescence images were acquired with an epifluorescence microscope (Olympus, X81).

Image-Pro Plus (v6.0) software was used to assess the total DAPI-positive nuclei number, Ki67-positive nuclei number, macrophage infiltrated area, human αvβ3 fluorescence intensity, murine β_3 fluorescence intensity and human GLUT-1. The Ki67 staining index (SI) was defined as the percentage of positive nuclei within the total number of nuclei. Human αvβ3 fluorescence intensity, murine β_3 fluorescence intensity, human GLUT-1, and macrophage infiltration intensity were calculated by measuring the integrated optical density (IOD) of images that were of equivalent area (mm^2). Tumor vasculature was evaluated by calculating the percentage of CD31 positive area divided by the total area of view. For each tumor section, ten random high-power images (20×) were analyzed.

Statistical analysis

Quantitative data were expressed as means ± SD. Means were compared using a Student's t test. P values <0.05 were considered statistically significant.

Results

$VEGF_{121}$/rGel treatment inhibited MDA-MB-435 tumor growth

Two doses of of $VEGF_{121}$/rGel, administered intraperitoneally (i.p.), were effective in delaying MDA-MB-435 tumor growth. As shown in Figure 1, a time-dependent increase in tumor volume was observed in the control group. The average tumor growth rates expressed as V/V_0, were 1.11 ± 0.07, 1.21 ± 0.10, 1.58 ± 0.36 and 2.64 ± 0.72 at days 1, 3, 7 and 14, respectively. Meanwhile, the $VEGF_{121}$/rGel treatment group showed V/V_0 ratios of 1.04 ± 0.06, 1.05 ± 0.11, 1.09 ± 0.17 and 1.86 ± 0.36 at days 1, 3, 7 and 14, respectively. A

significant difference in tumor volume was observed at day 7 between the treatment group and the control group ($p < 0.01$). At day 7, *i.e.* 4 days after withdrawal of the treatment, tumor growth resumed. There was no significant body weight loss observed during the treatment process, indicating that $VEGF_{121}$/rGel had no observable side effects at the dosage used during this study.

$VEGF_{121}$/rGel treatment showed no significant effect on glucose metabolism

Imaging of tumor metabolism with ^{18}F-FDG PET is an attractive approach for assessing the effects of therapy objectively and quantitatively.[1] ^{18}F-FDG PET scans of both $VEGF_{121}$/rGel treatment and PBS control groups of mice were acquired at days 0, 1, 3, 7 and 14. Typical coronal images are shown in Figure 2. Compared with the control group, no significant change of ^{18}F-FDG uptake in $VEGF_{121}$/rGel treated tumors was observed. The tumor $\%ID/g_{max}$ values in the treatment group were 11.2 ± 0.2, 12.4 ± 0.9, 12.7 ± 2.5, 10.2 ± 0.7 and 11.4 ± 0.9, respectively at days 0, 1, 3, 7 and day 14, while those in the control group remained unchanged throughout. Reduced or no signal toward the center of larger tumors is often observed, indicating the development of a central necrosis in these lesions.

Consistent with the ^{18}F-FDG PET imaging, no apparent differences in florescence intensity of GLUT-1 staining were detected in the $VEGF_{121}$/rGel therapy group, compared with the control group (Suppl. Figure 1A, B &, E). We also did not observe significant differences in florescence intensity of F4/80, a macrophage specific marker, in the $VEGF_{121}$/rGel therapy group compared with the control group (Suppl. Figure 1C, D &, F) at any time point.

$VEGF_{121}$/rGel treatment inhibited tumor cell proliferation

To evaluate VEGF121/rGel mediated changes of cellular proliferation, the same group of MDA-MB-435 tumor-bearing mice was injected with ^{18}F-FLT 8 h after the ^{18}F-FMISO scan. As shown in Figure 3, tumor uptake of ^{18}F-FLT decreased at both day 1 and day 3 after $VEGF_{121}$/rGel treatment, indicating that the drug inhibited tumor cell proliferation. Maximum tumor uptake ($\%ID/g_{max}$) calculated from PET images for the two groups (Figure 3B) revealed that the relative reduction in FLT uptake in treated tumors was approximately 13.0 ± 4.5%, compared to baseline, at day 1 and 25.0 ± 4.4% at day 3 ($n = 8$, $p < 0.01$). At day 7, *i.e.* 4 days after withdrawal of the treatment, FLT uptake was restored but somewhat less than the baseline level. The tumors in the control group showed a constant FLT uptake during the 2 week study period.

To further examine the relationship between FLT uptake and cell-cycle-related changes in the $VEGF_{121}$/rGel treated MDA-MB-435 tumor mice, the excised tumors were assayed by IHC for Ki67 expression. Examples of anti-Ki67 stained sections for the control and the $VEGF_{121}$/rGel treated tumors at days 1, 3, 7 and 14 are shown in Suppl. Figure 2. In the control tumor sections, a very high percentage of cells stained positively for Ki67 (Suppl. Figure 2A). In $VEGF_{121}$/rGel treated tumor sections, there was a clear reduction in the intensity of Ki67 staining as compared to the controls (Suppl. Figure 2B). The percentage of Ki67 positive cells (Ki67 staining index, SI) in untreated tumors was around 70 ± 5%, independent of the tumor size (Suppl. Figure 2C). No significantly delayed cell proliferation was observed in the $VEGF_{121}$/rGel treated mice at day 1 with a Ki67 SI of 56 ± 7% ($p > 0.05$), but there was a clear cell proliferation reduction at day 3 (37 ± 5%, $p < 0.01$) after $VEGF_{121}$/rGel treatment. The Ki67 SI was restored to the baseline level at day 7 and day 14 ($p > 0.05$), corroborating the *in vivo* ^{18}F-FLT imaging results.

$VEGF_{121}$/rGel treatment increased tumor hypoxia

To evaluate $VEGF_{121}$/rGel mediated changes of tumor hypoxia, MDA-MB-435 tumor-bearing mice were scanned with ^{18}F-FMISO. As shown in Figure 4, tumor uptake of ^{18}F-

FMISO increased at both day 1 and day 3 after $VEGF_{121}$/rGel treatment, indicating that the drug induced tumor hypoxia. Indeed, maximum tumor uptake (%ID/g_{max}) calculated from PET images for the two groups (Figure 4B) revealed that the relative enhancement in ^{18}F-FMISO uptake in the treated tumors was approximately 23.9 ± 15.7% as compared to the baseline at day 1 and 51.4 ± 29.4% at day 3 ($n = 8$, $p < 0.01$). At days 7 and 14, ^{18}F-FMISO uptake was restored to the baseline level. While the tumors in the control group showed no significant change.

$VEGF_{121}$/rGel treatment down regulated integrin αvβ3 expression

To determine the effects of $VEGF_{121}$/rGel treatment on tumor vasculature and tumor cell integrin expression, we performed PET scans utilizing the high affinity integrin radioligand ^{18}F-FPPRGD2. As shown in Figure 5, MDA-MB-435 tumors were clearly visualized on ^{18}F-FPPRGD2 PET images with clean background. In the control tumors, ^{18}F-FPPRGD2 uptake was stable between days 0 and 14. In $VEGF_{121}$/rGel treated tumors, ^{18}F-FPPRGD2 uptake decreased significantly at day 1 by 23.9 ± 8.8 % ($p < 0.05$) and at day 3 by 36.3 ± 9.2 % ($p < 0.01$), relative to the baseline, then slowly recovered to the baseline level at day 14 (Figure 5B).

To further investigate the mechanism of altered ^{18}F-FPPRGD2 uptake during and after VEGF121/rGel treatment, we stained tumor sections with anti-murine integrin β3 and anti-human integrin αvβ3 antibodies. As shown in Suppl. Figure 3, MDA-MB-435 tumor had positive human integrin αvβ3 staining. However, we did not observe apparent changes of the human integrin αvβ3 staining florescence intensity after $VEGF_{121}$/rGel treatment, indicating the change of tumor uptake of ^{18}F-FPPRGD2 was not related to integrin expression on tumor cells. Tumor vasculature was of murine origin and the expression of murine integrin β3 was mainly on the tumor vascular endothelial cells, so the fluorescent signal from murine β3 was co-localized with that of murine CD31 (Figure 6). The median murine β3 florescence intensity was 0.025 ± 0.0016 in the control group, which was decreased significantly to 0.017 ± 0.0016 at day 1 ($p < 0.05$) and 0.016 ± 0.002 at day 3 ($p < 0.05$) in the $VEGF_{121}$/rGel treated group (Figure 6B and F). At day 7 and day 14, the mean florescence intensity in the $VEGF_{121}$/rGel treated group was increased to 0.022 ± 0.0017 and 0.024 ± 0.0028, with no significant difference when compared with control group ($p > 0.05$), which correlated well with the ^{18}F-FPPRGD2 imaging studies.

MDA-MB-435 tumors have abundant vasculature, as indicated by strong CD31 staining in all of the untreated MDA-MB-435 tumor sections (Figure 6A). Significant changes of vascular morphology between the $VEGF_{121}$/rGel treated group and the control group at different time points were observed. For example, the blood vessels in the control group were much dilated and microvessel cavities could be identified, while the microvessel cavity was collapsed in $VEGF_{121}$/rGel treated tumors, especially at day 1 and day 3 after treatment (Figure 6A). Based on CD31 staining, we also quantified vascular area in $VEGF_{121}$/rGel treated and control tumors. As shown in Figure 6E, the percentage of vascular area significantly decreased to 4.3 ± 0.4% at day1 after $VEGF_{121}$/rGel treatment compared with the control group (9.4 ± 1.3%, $p < 0.05$) and even lower at day 3 (3.1 ± 0.6%, $p < 0.05$). However, no significant difference was detected at day 7 and day 14 ($p > 0.05$).

Discussion

To circumvent the limitations of anatomic imaging in evaluating therapeutic responses to cytostatic agents, including anti-angiogenic therapeutics, we applied multiplexed PET probes to MDA-MB-435 human breast cancer model to monitor the tumor response to $VEGF_{121}$/rGel treatment. The short half life of ^{18}F ($t_{1/2}$= 109.8 min) makes it feasible to acquire two sets of PET images on the same batch of animals on the same day at 8 h

interval. Indeed, Dandekar *et al.* performed same-day ^{18}F-FDG PET scans on the same mice with B16F10 murine melanoma xenografts at a 6 h interval after reinjection of ^{18}F-FDG. The mean %ID/g values of the first set of scans and the second set of scans were not significantly different ($p > 0.44$).[17] In order to minimize the influence of the first set of scans (^{18}F-FPPRGD2 and ^{18}F-FMISO) on the second set of scans (^{18}F-FDG and ^{18}F-FLT), we also controlled the injection dose of ^{18}F-FPPRGD2 and ^{18}F-FMISO to be around 1.1 MBq (30 μCi), instead of the 3.7–7.4 MBq (100–200 μCi) typically used in the previous studies.[17]

^{18}F-FDG has been widely used both pre-clinically and clinically to monitor tumor glucose metabolism. Although treatment monitoring with ^{18}F-FDG PET may have a significant impact on patient management in several clinical situations, published data on the accuracy of ^{18}F-FDG PET in specific clinical situations often appear heterogeneous.[1] Moreover, in a clinical trial of recombinant human endostatin (rh-Endo), metabolism as measured by PET scans showed no correlation with increased dose of rh-Endo,[18] indicating the limitation of ^{18}F-FDG PET in evaluation of therapeutic responses to anti-angiogenic agents. Similarly, ^{18}F-FDG PET did not have significant change upon VEGF$_{121}$/rGel treatment in the current study.

We have previously demonstrated that 4 total doses of 24 mg/kg VEGF$_{121}$/ rGel specifically targeted and damaged glioblastoma neovasculature, resulting in decreased tumor DNA synthesis, increased apoptosis, and overall decreased tumor growth (*8*). In order to monitor the early response of tumor to VEGF$_{121}$/rGel therapy, we treated the MDA-MB-435 tumor-bearing mice with 2 doses of drug instead of 4 doses in this study. We observed initial tumor growth inhibition and then re-growth a few days after the cease of the treatment. The tumor growth inhibition was supported by decreased Ki67 SI in VEGF$_{121}$/rGel treated tumors. The anti-proliferation effect of VEGF$_{121}$/rGel was further demonstrated by decreased ^{18}F-FLT uptake, especially at day 3 after the treatment ($p < 0.01$) (Figure 3), suggesting the potential of ^{18}F-FLT PET to monitor tumor response to cancer therapy.[19–20]

Most solid tumors show evidence of hypoxia, presumably as a consequence of tumor cell proliferation outpacing neoangiogenesis.[21] In turn, hypoxia is a key mediator of angiogenesis, at least in part because it induces the expression of VEGF. PET studies using ^{18}F-FMISO, which is retained in hypoxic cells through an electron transfer that prevents its egress from cells,[22] have demonstrated variable, but significant levels of hypoxia in various types of tumors, such as soft-tissue sarcomas,[23–25] breast cancer,[26–27] and glioblastoma.[28] Different from cytotoxic agents that would destroy cancer cells directly, the antiangiogenic agents target cancer cells indirectly by depriving them of nutrients and oxygen. Indeed, within 48 h of i.v. administration, vascular damage and thrombosis of tumor blood vessels have been observed in VEGF$_{121}$/rGel treated tumors, due to cytotoxicity on KDR positive tumor vascular endothelial cells.[5] The vasculature damage in this study also was confirmed by CD31 staining on tumor sections (Figure 6). We also performed longitudinal PET scans with ^{18}F-FMISO to evaluate VEGF$_{121}$/rGel induced hypoxia. Not surprisingly, we observed significantly increased ^{18}F-FMISO uptake in VEGF$_{121}$/rGel treated tumors at both day 1 and day 3 after treatment, indicating that the drug induced tumor hypoxia (Figure 4). With both ^{18}F-FDG and ^{18}F-FLT PET, we have identified central necrosis among tumors, especially at day 14 when tumor size is relatively big. Theoretically, chronic hypoxia would present at the peripheral regions of the necrotic centers. However, no significant difference of ^{18}F-FMISO uptake were observed, which may be due to the variability of PET imaging and inadequate animal numbers.[17] The increased tumor uptake of ^{18}F-FMSIO observed in VEGF$_{121}$/rGel treated tumors was highly likely a result of acute hypoxia caused by collapsed tumor vasculature.

The integrin avβ3 receptor is upregulated on tumor vascular endothelial cells and plays important roles in angiogenesis and metastasis. Thus, non-invasive visualization and quantification of integrin αvβ3 expression levels *in vivo* should provide useful information about tumor response to $VEGF_{121}$/rGel treatment. A series of radiolabeled RGD monomers and multimers have been developed for imaging integrin αvβ3 expression and there have been several reports of using these RGD peptide tracers to monitor chemotherapy and/or anti-angiogenic treatment efficacy. For example, reduction of tumor glucosamino ^{99m}Tc-D-c(RGDfK) uptake, as determined by γ-camera imaging was observed in paclitaxel treated Lewis lung carcinoma (LLC) tumor-bearing.[29] It has also been reported that the uptake of ^{18}F-AH111585 in Calu-6 tumors was reduced significantly after 3 doses (100 mg/kg) of ZD4190 (a tyrosine kinase inhibitor) treatment.[30] Compared with ^{18}F-AH111585 and ^{18}F-Galacto-RGD, the dimeric peptide ^{18}F-FPPRGD2 showed relatively high tumor integrin-specific accumulation and favorable *in vivo* kinetics.[12,30–32]

In our study, ^{18}F-FPPRGD2 uptake in the untreated tumors remained unchanged throughout the therapy and imaging process. In $VEGF_{121}$/rGel treated tumors, the uptake was decreased by 24% and 36% at day 1 and 3 respectively, then resumed to the baseline level at day 14. Fluorescence immunostaining against murine integrin β3, which is supposed to be expressed on tumor vascular endothelial cells and colocalized with murine CD31, revealed that mean murine β3 florescence intensity was decreased significantly at day 1 and day 3 ($p < 0.05$) (Figure 6) after $VEGF_{121}$/rGel treatment, which was consistent with the dynamic pattern of the ^{18}F-FPPRGD2 PET. Besides tumor vascular endothelial cells, MDA-MB-435 tumor cells also express integrin αvβ3 of human origin, which should be recognized and visualized by ^{18}F-FPPRGD2. We performed immunostaining against human integrin αvβ3 and found no apparent change of integrin expression level on tumor cells, which is consistent with a previous report and our own finding.[14, 33] Thus, we speculated that the change of ^{18}F-FPPRGD2 uptake reflected the change of tumor vascular integrin level upon $VEGF_{121}$/rGel treatment, rather than tumor cell integrin expression. We also noticed that changes of tumor uptake of ^{18}F-FMISO and ^{18}F-FPPRGD2 were in opposite directions, indicating that the tumor uptake of ^{18}F-FPPRGD2 might be affected at least partially by decreased tumor blood supply and hypoxia.

With multiplexed longitudinal PET imaging, we monitored several key aspects of tumor biology including glucose metabolism, cellular proliferation, hypoxia, and angiogenesis, with ^{18}F-FDG, ^{18}F-FLT, ^{18}F-FMISO, and ^{18}F-FPPRGD2 as the imaging tracers. At early time points (day 1 and day 3) following $VEGF_{121}$/rGel treatment, ^{18}F-FLT, ^{18}F-FPPRGD2 and ^{18}F-FMISO PET all showed significant changes in tumor uptake, while ^{18}F-FDG PET revealed no significant difference between the control group and the treated group. The magnitudes of PET signal alterations of ^{18}F-FPPRGD2 (decrease) and ^{18}F-FMISO (increase) were higher than that of the ^{18}F-FLT (decrease), indicating the superiority of hypoxia and angiogenesis imaging strategies over proliferation imaging in reflecting early tumor response to anti-angiogenic therapeutics such as $VEGF_{121}$/rGel.

In conclusion, we have demonstrated the feasibility of using multiplexed PET imaging probes to monitor early tumor responses to $VEGF_{121}$/rGel therapy in different aspects of tumor biology. The results showed that ^{18}F-FLT, ^{18}F-FMISO and ^{18}F-FPPRGD2 are superior to ^{18}F-FDG in monitoring therapy response, as supported by *ex vivo* analyses of related biomarkers. This pre-clinical study should be helpful in accelerating anti-cancer drug development and promoting the clinical translation of molecular imaging.

Supplementary Material

Refer to Web version on PubMed Central for supplementary material.

Acknowledgments

This project was supported by the Intramural Research Program of the National Institute of Biomedical Imaging and Bioengineering (NIBIB), National Institutes of Health (NIH) and the International Cooperative Program of National Science Foundation of China (NSFC) (81028009). Min Yang is partly supported by the Outstanding Professionals Foundation of Jiangsu Health Bureau (Grant No. RC 2007096). Gang Niu currently is an Imaging Sciences Training Program (ISTP) Fellow, jointly supported by the Radiology and Imaging Sciences Department, NIH Clinical Center and the Intramural Research Program, NIBIB, NIH. We acknowledge the NIH/CC cyclotron facility for isotope production and Dr. Henry S. Eden for proof-reading this manuscript.

References

1. Weber WA. Assessing tumor response to therapy. J Nucl Med. 2009; 50 Suppl 1:1S–10S. [PubMed: 19380403]
2. Moertel CG, Hanley JA. The effect of measuring error on the results of therapeutic trials in advanced cancer. Cancer. 1976; 38(1):388–394. [PubMed: 947531]
3. Eisenhauer EA, Therasse P, Bogaerts J, Schwartz LH, Sargent D, Ford R, Dancey J, Arbuck S, Gwyther S, Mooney M, Rubinstein L, Shankar L, Dodd L, Kaplan R, Lacombe D, Verweij J. New response evaluation criteria in solid tumours: revised RECIST guideline (version 1.1). Eur J Cancer. 2009; 45(2):228–247. [PubMed: 19097774]
4. Michalski MH, Chen X. Molecular imaging in cancer treatment. Eur J Nucl Med Mol Imaging. 2011; 38(2):358–377. [PubMed: 20661557]
5. Veenendaal LM, Jin H, Ran S, Cheung L, Navone N, Marks JW, Waltenberger J, Thorpe P, Rosenblum MG. In vitro and in vivo studies of a VEGF121/rGelonin chimeric fusion toxin targeting the neovasculature of solid tumors. Proc Natl Acad Sci U S A. 2002; 99(12):7866–7871. [PubMed: 12060733]
6. Akiyama H, Mohamedali KA, RL ES, Kachi S, Shen J, Hatara C, Umeda N, Hackett SF, Aslam S, Krause M, Lai H, Rosenblum MG, Campochiaro PA. Vascular targeting of ocular neovascularization with a vascular endothelial growth factor121/gelonin chimeric protein. Mol Pharmacol. 2005; 68(6):1543–1550. [PubMed: 16150930]
7. Ran S, Mohamedali KA, Luster TA, Thorpe PE, Rosenblum MG. The vascular-ablative agent $VEGF_{121}$/rGel inhibits pulmonary metastases of MDA-MB-231 breast tumors. Neoplasia. 2005; 7(5):486–496. [PubMed: 15967101]
8. Hsu AR, Cai W, Veeravagu A, Mohamedali KA, Chen K, Kim S, Vogel H, Hou LC, Tse V, Rosenblum MG, Chen X. Multimodality molecular imaging of glioblastoma growth inhibition with vasculature-targeting fusion toxin $VEGF_{121}$/rGel. J Nucl Med. 2007; 48(3):445–454. [PubMed: 17332623]
9. Weber WA, Czernin J, Phelps ME, Herschman HR. Technology Insight: novel imaging of molecular targets is an emerging area crucial to the development of targeted drugs. Nat Clin Pract Oncol. 2008; 5(1):44–54. [PubMed: 18097456]
10. Lee SJ, Oh SJ, Chi DY, Kil HS, Kim EN, Ryu JS, Moon DH. Simple and highly efficient synthesis of 3'-deoxy-3'-[^{18}F]fluorothymidine using nucleophilic fluorination catalyzed by protic solvent. Eur J Nucl Med Mol Imaging. 2007; 34(9):1406–1409. [PubMed: 17384949]
11. Tang G, Wang M, Tang X, Gan M, Luo L. Fully automated one-pot synthesis of [^{18}F]fluoromisonidazole. Nucl Med Biol. 2005; 32(5):553–558. [PubMed: 15982586]
12. Liu S, Liu Z, Chen K, Yan Y, Watzlowik P, Wester HJ, Chin FT, Chen X. 18F-labeled galacto and PEGylated RGD dimers for PET imaging of αvβ3 integrin expression. Mol Imaging Biol. 2010; 12(5):530–538. [PubMed: 19949981]
13. Mohamedali KA, Kedar D, Sweeney P, Kamat A, Davis DW, Eve BY, Huang S, Thorpe PE, Dinney CP, Rosenblum MG. The vascular-targeting fusion toxin $VEGF_{121}$/rGel inhibits the growth of orthotopic human bladder carcinoma tumors. Neoplasia. 2005; 7(10):912–920. [PubMed: 16242074]
14. Sun X, Yan Y, Liu S, Cao Q, Yang M, Neamati N, Shen B, Niu G, Chen X. ^{18}F-FPPRGD2 and ^{18}F-FDG PET of Response to Abraxane Therapy. J Nucl Med. 2011; 52(1):140–146. [PubMed: 21149494]

15. Jacobs AH, Thomas A, Kracht LW, Li H, Dittmar C, Garlip G, Galldiks N, Klein JC, Sobesky J, Hilker R, Vollmar S, Herholz K, Wienhard K, Heiss WD. ^{18}F-fluoro-L-thymidine and ^{11}C-methylmethionine as markers of increased transport and proliferation in brain tumors. J Nucl Med. 2005; 46(12):1948–1958. [PubMed: 16330557]
16. Liu RS, Chou TK, Chang CH, Wu CY, Chang CW, Chang TJ, Wang SJ, Lin WJ, Wang HE. Biodistribution, pharmacokinetics and PET imaging of [^{18}F]FMISO, [^{18}F]FDG and [^{18}F]FAc in a sarcoma- and inflammation-bearing mouse model. Nucl Med Biol. 2009; 36(3):305–312. [PubMed: 19324276]
17. Dandekar M, Tseng JR, Gambhir SS. Reproducibility of ^{18}F-FDG microPET studies in mouse tumor xenografts. J Nucl Med. 2007; 48(4):602–607. [PubMed: 17401098]
18. Herbst RS, Mullani NA, Davis DW, Hess KR, McConkey DJ, Charnsangavej C, O'Reilly MS, Kim HW, Baker C, Roach J, Ellis LM, Rashid A, Pluda J, Bucana C, Madden TL, Tran HT, Abbruzzese JL. Development of biologic markers of response and assessment of antiangiogenic activity in a clinical trial of human recombinant endostatin. J Clin Oncol. 2002; 20(18):3804–3814. [PubMed: 12228200]
19. Sohn HJ, Yang YJ, Ryu JS, Oh SJ, Im KC, Moon DH, Lee DH, Suh C, Lee JS, Kim SW. [^{18}F]Fluorothymidine positron emission tomography before and 7 days after gefitinib treatment predicts response in patients with advanced adenocarcinoma of the lung. Clin Cancer Res. 2008; 14(22):7423–7429. [PubMed: 19010859]
20. de Langen AJ, Klabbers B, Lubberink M, Boellaard R, Spreeuwenberg MD, Slotman BJ, de Bree R, Smit EF, Hoekstra OS, Lammertsma AA. Reproducibility of quantitative ^{18}F-3'-deoxy-3'-fluorothymidine measurements using positron emission tomography. Eur J Nucl Med Mol Imaging. 2009; 36(3):389–395. [PubMed: 18931838]
21. Dubois L, Landuyt W, Haustermans K, Dupont P, Bormans G, Vermaelen P, Flamen P, Verbeken E, Mortelmans L. Evaluation of hypoxia in an experimental rat tumour model by [^{18}F]fluoromisonidazole PET and immunohistochemistry. Br J Cancer. 2004; 91(11):1947–1954. [PubMed: 15520822]
22. Padhani AR, Krohn KA, Lewis JS, Alber M. Imaging oxygenation of human tumours. Eur Radiol. 2007; 17(4):861–872. [PubMed: 17043737]
23. Brizel DM, Rosner GL, Harrelson J, Prosnitz LR, Dewhirst MW. Pretreatment oxygenation profiles of human soft tissue sarcomas. Int J Radiat Oncol Biol Phys. 1994; 30(3):635–642. [PubMed: 7928495]
24. Nordsmark M, Loncaster J, Chou SC, Havsteen H, Lindegaard JC, Davidson SE, Varia M, West C, Hunter R, Overgaard J, Raleigh JA. Invasive oxygen measurements and pimonidazole labeling in human cervix carcinoma. Int J Radiat Oncol Biol Phys. 2001; 49(2):581–586. [PubMed: 11173158]
25. Fyles A, Milosevic M, Hedley D, Pintilie M, Levin W, Manchul L, Hill RP. Tumor hypoxia has independent predictor impact only in patients with node-negative cervix cancer. J Clin Oncol. 2002; 20(3):680–687. [PubMed: 11821448]
26. Knowles HJ, Phillips RM. Identification of differentially expressed genes in experimental models of the tumor microenvironment using differential display. Anticancer Res. 2001; 21(4A):2305–2311. [PubMed: 11724287]
27. Mankoff DA, Dunnwald LK, Gralow JR, Ellis GK, Charlop A, Lawton TJ, Schubert EK, Tseng J, Livingston RB. Blood flow and metabolism in locally advanced breast cancer: relationship to response to therapy. J Nucl Med. 2002; 43(4):500–509. [PubMed: 11937594]
28. Valk PE, Mathis CA, Prados MD, Gilbert JC, Budinger TF. Hypoxia in human gliomas: demonstration by PET with fluorine-18-fluoromisonidazole. J Nucl Med. 1992; 33(12):2133–2137. [PubMed: 1334136]
29. Jung KH, Lee KH, Paik JY, Ko BH, Bae JS, Lee BC, Sung HJ, Kim DH, Choe YS, Chi DY. Favorable biokinetic and tumor-targeting properties of ^{99m}Tc-labeled glucosamino RGD and effect of paclitaxel therapy. J Nucl Med. 2006; 47(12):2000–2007. [PubMed: 17138743]
30. Morrison MS, Ricketts SA, Barnett J, Cuthbertson A, Tessier J, Wedge SR. Use of a novel Arg-Gly-Asp radioligand, ^{18}F-AH111585, to determine changes in tumor vascularity after antitumor therapy. J Nucl Med. 2009; 50(1):116–122. [PubMed: 19091899]

31. McParland BJ, Miller MP, Spinks TJ, Kenny LM, Osman S, Khela MK, Aboagye E, Coombes RC, Hui AM, Cohen PS. The biodistribution and radiation dosimetry of the Arg-Gly-Asp peptide ^{18}F-AH111585 in healthy volunteers. J Nucl Med. 2008; 49(10):1664–1667. [PubMed: 18794263]

32. Beer AJ, Haubner R, Wolf I, Goebel M, Luderschmidt S, Niemeyer M, Grosu AL, Martinez MJ, Wester HJ, Weber WA, Schwaiger M. PET-based human dosimetry of ^{18}F-galacto-RGD, a new radiotracer for imaging αvβ3 expression. J Nucl Med. 2006; 47(5):763–769. [PubMed: 16644745]

33. Dumont RA, Hildebrandt I, Su H, Haubner R, Reischl G, Czernin JG, Mischel PS, Weber WA. Noninvasive imaging of αvβ3 function as a predictor of the antimigratory and antiproliferative effects of dasatinib. Cancer Res. 2009; 69(7):3173–3179. [PubMed: 19318569]

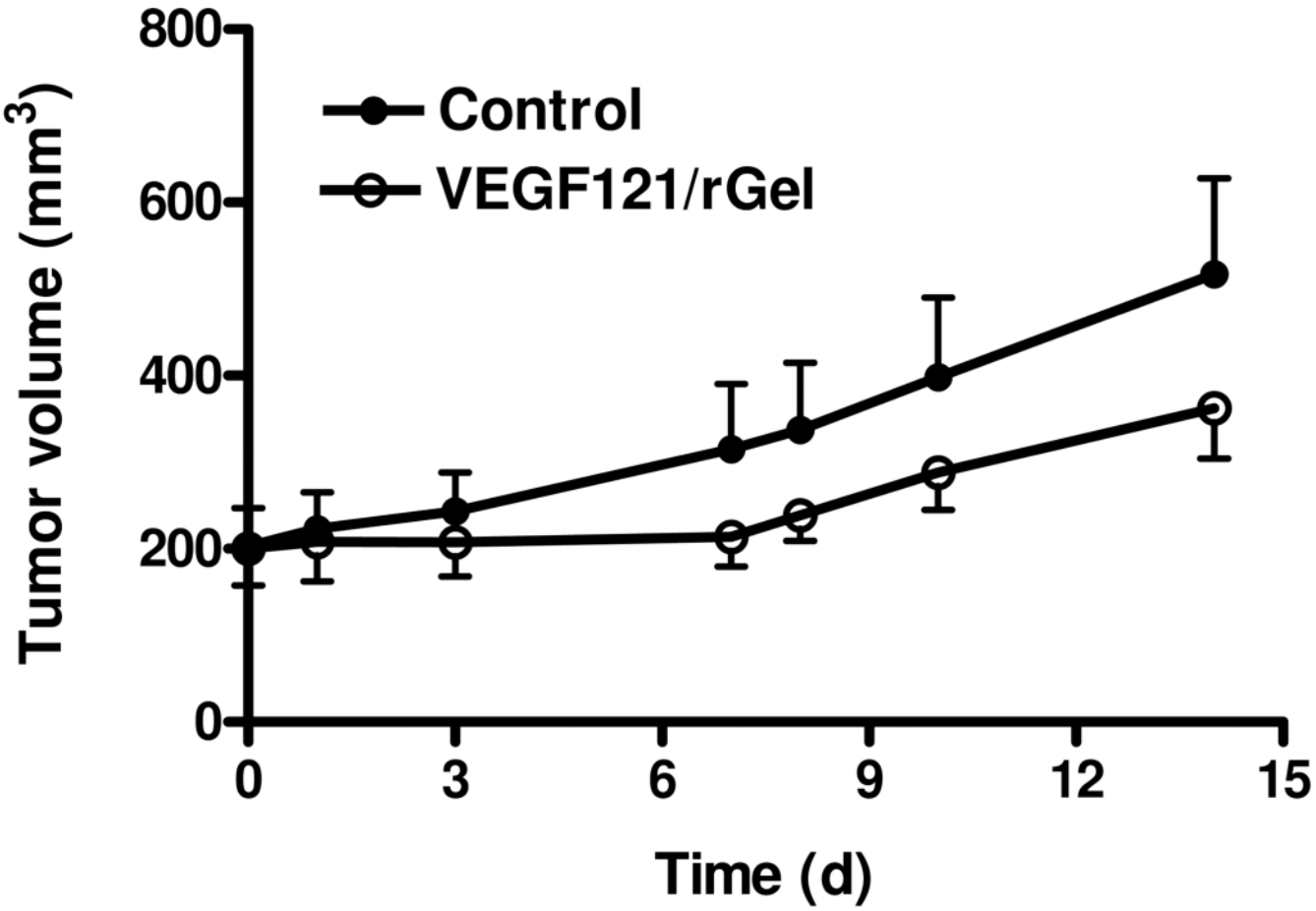

Figure 1.
Antitumor activity of $VEGF_{121}$/rGel in MDA-MB-435 breast cancer model. Two doses of $VEGF_{121}$/rGel (12 mg/kg on day 1, and day 3, i.p.) inhibited tumor growth.

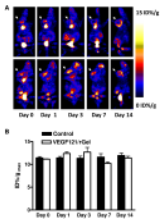

Figure 2.

(A) Representative decay-corrected whole-body coronal microPET images of mice bearing MDA-MB-435 breast cancer at 1 h after intravenous injection of ^{18}F-FDG (1.85 MBq/mouse) on days 0, 1, 3, 7 and 14 after the treatment was initiated. The tumors are indicated by arrows. Upper panel: control; Lower panel: $VEGF_{121}$/rGel treatment. (B) Tumor uptake of ^{18}F-FDG quantified by ROI analysis.

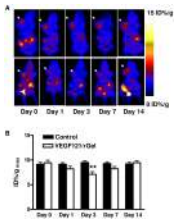

Figure 3.

(A) Representative decay-corrected whole-body coronal microPET images of mice bearing MDA-MB-435 breast cancer at 1.5 h after intravenous injection of ^{18}F-FLT (1.85 MBq/mouse) on days 0, 1, 3, 7 and 14 after the treatment was initiated. The tumors are indicated by arrows. Decreased uptake of ^{18}F-FLT was observed on day 1 and day 3 but resumed to baseline level on day 7. Upper panel: control; Lower panel: $VEGF_{121}$/rGel treatment. (B) Quantitative microPET region of interest analysis of tumor uptake for ^{18}F-FLT. (** $p < 0.01$)

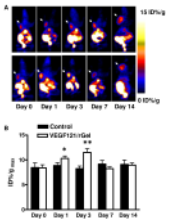

Figure 4.

(A) Representative decay-corrected whole-body coronal microPET images of mice bearing MDA-MB-435 breast cancer at 2.5 h after intravenous injection of ^{18}F-FMISO (1.11 MBq/mouse) on days 0, 1, 3, 7 and 14 after the treatment was initiated. The tumors are indicated by arrows. Increased tumor uptake of ^{18}F-FMISO was observed on day 1 and day 3 but was restored to the baseline level on day 7. Upper panel: control; Lower panel: $VEGF_{121}$/rGel treatment. (B) Quantitative microPET region of interest analysis of tumor uptake for ^{18}F-FMISO. (* $p < 0.05$, ** $p < 0.01$)

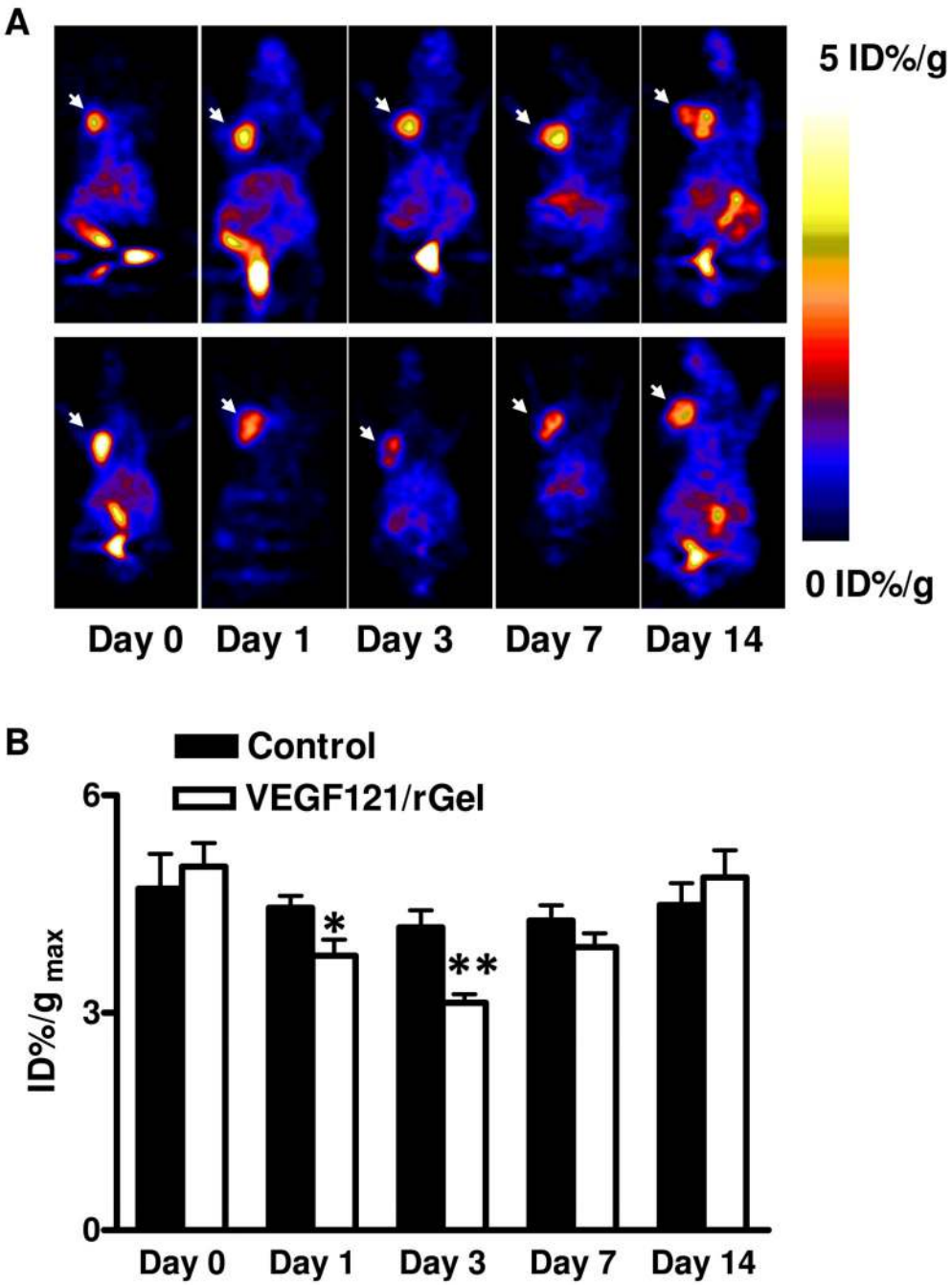

Figure 5.

(A) Representative decay-corrected whole-body coronal microPET images of mice bearing MDA-MB-435 breast cancer at 1 h after intravenous injection of ^{18}F-FPPRGD2 (1.11 MBq/mouse) on days 0, 1, 3, 7 and 14 after the treatment was initiated. The tumors are indicated by arrows. Decreased tumor uptake of ^{18}F-FPPRGD2 was observed on day 1 and day 3 but was restored to the baseline level on day 14. Upper panel: control; Lower panel: $VEGF_{121}$/rGel treatment. (B) Quantitative microPET region of interest analysis of tumor uptake for ^{18}F-FPPRGD2. (* $p < 0.05$, ** $p < 0.01$)

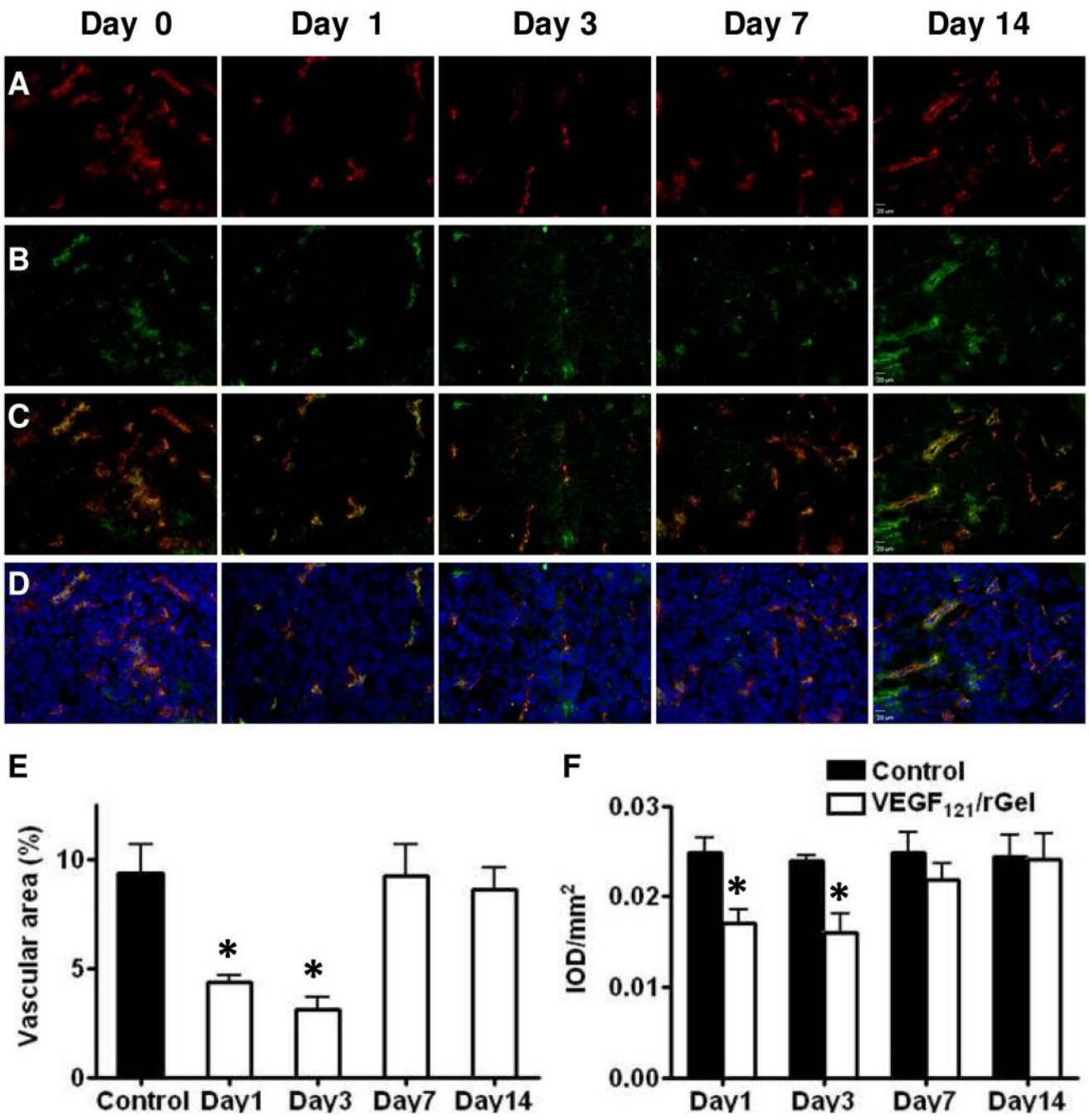

Figure 6.

Immunofluorescence staining of tumor vasculature and murine integrin β3 expression. (A) CD31 (red); (B) CD61 (green). (C) Overlay of CD31 and CD61; (D) Overlay of CD31 and CD61 plus DAPI (Blue); (E) Calculated vascular area based on CD31 staining (* $p < 0.05$); (F) CD61 integrated optical density was plotted in the histogram. (* $p < 0.05$).

Table 1

Experimental Design for longitudinal, multiplexed PET imaging of $VEGF_{121}$/rGel treatment efficacy, and ex vivo histopathology.

		Day 0	Day 1	Day 3	Day 7	Day 14
^{18}F-FPPRGD2	Control	#	+ #	+ #	#	#
	$VEGF_{121}$/rGel	#	+ #	+ #	#	#
^{18}F-FDG	Control	#	+ #	+ #	#	#
	$VEGF_{121}$/rGel	#	+ #	+#	#	#
^{18}F-FMISO	Control	#	+ #	+ #	#	#
	$VEGF_{121}$/rGel	#	+ #	+ #	#	#
18F-FLT	Control	#	+ #	+ #	#	#
	VEGF121/rGel	#	+ #	+ #	#	#
Histology		-	-	-	-	-

#, microPET imaging; +, Control Vehicle or $VEGF_{121}$/rGel treatment; −, Tumor tissue sampling; ^{18}FFPPRGD2 and ^{18}F-FDG PET imaging studies were performed on the same day with the same group of animals at 8 h interval (^{18}F-FPPRGD2 PET first and ^{18}F-FDG PET 8 h later); ^{18}F-FMISO and ^{18}F-FLT PET images were performed on the same day with the same group of animals (^{18}F-FMISO PET first and ^{18}FFLT PET 8 h later).